

On the dependency of rubber friction on the normal force or load: theory and experiment

G. Fortunato, V. Ciaravola, and A. Furno

Bridgestone Technical Center Europe, Via del Fosso del Salceto 13/15 00128 Roma

M. Scaraggi

DII, Universit del Salento, 73100 Monteroni-Lecce, Italy, EU and

PGI, FZ-Jülich, 52425 Jülich, Germany, EU

B. Lorenz and B.N.J. Persson

PGI, FZ-Jülich, 52425 Jülich, Germany, EU and

w.MultiscaleConsulting.com

In rubber friction studies it is often observed that the kinetic friction coefficient μ depends on the nominal contact pressure p . We discuss several possible origins of the pressure dependency of μ : (a) saturation of the contact area (and friction force) due to high nominal squeezing pressure, (b) non-linear viscoelasticity, (c) non-randomness in the surface topography, in particular the influence of the skewness of the surface roughness profile, (d) adhesion, and (e) frictional heating. We show that in most cases the non-linearity in the $\mu(p)$ relation is mainly due to process (e) (frictional heating), which softens the rubber, increases the area of contact, and (in most cases) reduces the viscoelastic contribution to the friction. In fact, since the temperature distribution in the rubber at time t depends on the sliding history (i.e., on the earlier time $t' < t$), the friction coefficient at time t will also depend on the sliding history, i.e. it is, strictly speaking, a time integral operator.

The energy dissipation in the contact regions between solids in sliding contact can result in high local temperatures which may strongly affect the area of real contact and the friction force (and the wear-rate). This is the case for rubber sliding on road surfaces at speeds above 1 mm/s. In Ref. [14] we have derived equations which describe the frictional heating for solids with arbitrary thermal properties. In this paper the theory is applied to rubber friction on road surfaces. Numerical results are presented and compared to experimental data. We observe good agreement between the calculated and measured temperature increase.

1 Introduction

The Coulomb friction law states that the friction force is proportional to the normal force or load, and is found to hold remarkable well in many practical applications[1, 2]. The assumption that the friction coefficient is independent of the nominal contact pressure is often used also in rubber friction applications, e.g., in classical Finite Element Method (FEM) calculations, where the relation is usually written as a relation between the local frictional shear stress $\tau(x, y)$ and the local contact pressure $p(x, y)$:

$$\tau(x, y) = \mu p(x, y). \quad (1)$$

Here it is implicitly assumed that the surfaces can be treated as smooth, but may have a macroscopic curvature (say with the radius of curvature R). This approach assumes that the longest wavelength roughness components on the surfaces is short compared to the size of the nominal contact region, and also compared to the length scale R associated with the macroscopic curvature. In that case the frictional shear stress $\tau(x, y)$ and contact pressure $p(x, y)$ in (1) must be considered as the locally average of the corresponding microscopic quantities, which may vary rapidly in space down to length scales of order an atomic distance.

In tire applications it is usually found that increasing the load results in a reduction of the effective friction coefficient (e.g., a reduction in the maximum of the μ -slip curve). This is usually interpreted as a dependency of the friction coefficient on the nominal contact pressure. However, increasing the normal load also changes the tire-road footprint, which affect the tire-road friction. Thus, as will be shown in Sec. 7, an increase in the length of the tire-road footprint (as a result of an increase in the tire load), usually results in a reduction of the maximum of the μ -slip curve[3, 4].

In this paper we will discuss different processes which result in a pressure dependency of the friction coefficient μ : (a) saturation of the contact area (and friction force) due to high nominal squeezing pressure, (b) non-linear viscoelasticity, (c) non-randomness in the surface topography, in particular the influence of skewness of the surface roughness profile, (d) adhesion, and (e) frictional heating. We find that the latter mechanism is most important in tire applications and in what follows we will focus mainly on this case.

When a rectangular block with nominally smooth surface is squeezed in contact with a nominally flat substrate, because of surface roughness the area of real contact is usually only a very small fraction of the nominal contact area. For hard solids the contact pressure in the

area of real contact will therefore be very high. During sliding frictional energy dissipation will take place in the area of real contact and because of the small volumes involved, at high enough sliding speed where thermal diffusion becomes unimportant, the local (flash) temperatures may be very high. As a result local melting of the material, or other phase transformations, can take place. In addition tribochemical reactions, and emission of photons or other particles, may occur at or in the vicinity of the contact regions. All these processes will also affect the friction force, e.g., if frictional melting occurs the melted film may act as a lubricant and lower the friction as is the case, e.g., when sliding on ice or snow at high enough velocity. It is clear that a deep understanding of the role of frictional heating is of crucial importance in many cases for understanding friction and wear processes.

Pioneering theoretical works on the temperature distribution in sliding contacts have been presented by Jaeger[5], Archard[6] and others[7–11]. In these studies a moving heat source is located at the sliding interface. However, some materials like rubber have internal friction and when such solids are sliding on a rough surface frictional energy will be dissipated not just at the sliding interface but also some distance into the viscoelastic material. The flash temperature effect related to this process was studied in Ref. [12], but neglecting the contribution from the frictional interaction between the surfaces in the area of real contact, and also neglecting heat transfer to the substrate. In Ref. [13] the theory of [12] was extended to include these effects, but assuming that the substrate has infinite thermal conductivity. In Ref. [14] we remove this last restriction and present a general theory of frictional heating, which we will use in this paper (see Sec. 6).

There are many experimental studies of the temperature in frictional contacts, e.g., see Ref. [15]. When analyzing experimental data it is usually assumed that the temperature is continuous at the rubber-substrate interface. However, the latter assumption is in general not valid, in particular if surface roughness exist and the contact area is incomplete within the nominal contact region. One needs to use a heat transfer description[2, 16–22] which relates the temperature jump $T_R - T_S$ between the rubber surface (T_R) and the substrate surface (T_S) to the heat current J through the interface via $J = \alpha(T_R - T_S)$, where the heat transfer coefficient α in general depends on the sliding speed[13]. We used this more general approach in Ref. [14] and also in this paper.

2 Contact mechanics theory: short review

Nearly all surfaces have roughness, usually extending from the linear size of the object down to atomistic length scales, say from cm to nm. This may involve ~ 7 decades in length scales corresponding to $\sim 10^{21}$ degrees of freedom. The contact between solids with surface roughness cannot therefore in general be studied numerically

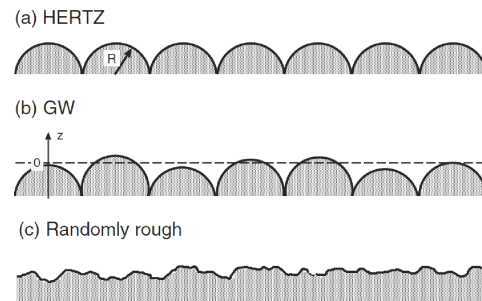


Figure 1: Three different models of a “rough” surface. In case (a) all the asperities are equally high and have identical radius of curvature. Introducing asperities with a random height distribution as in (b) gives the Greenwood-Williamson approach towards contact mechanics. In (c) a real, randomly rough surface is shown, where the asperities are of different heights and curvature radii.

on all relevant length scales without further simplifications. Thus, it is very important to develop analytical approaches to the contact between solids with rough surfaces.

Contact mechanics has a very long history[23]. The first study was presented by Hertz in 1882 (*Über die Berührung fester elastischer Körper*), where he studied the frictionless contact between elastic solids with smooth surface profiles which could be approximated as parabolic close to the contact area. This theory predicts a nonlinear increase of the contact area A with the squeezing force F . The most simple model of a rough surface consists of a regular array of spherical bumps with equal radius of curvature R and equal height (see Fig. 1(a)). If such a surface gets squeezed against an elastic solid with a flat surface, one can approximately apply the Hertz contact theory to each asperity. Thus, from this simple approach one expects that the real area of contact will scale nonlinearly with F . However, this is not in accordance with experiments which show that the real area of contact is proportional to F as long as the contact area $A \ll A_0$, where A_0 is the nominal contact area. This is also the reason for why the friction force is usually proportional to the load (Coulomb friction law).

Greenwood and Williamson (GW) proposed that the contact problem between two elastic rough surfaces could be reduced to the problem of one infinitely-hard rough surface acting on a flat elastic countersurface. Within their model, the rough topography was described by a large collection of hemispherical asperities of uniform radius (which individually satisfied the Hertzian approximation) with a height distribution that followed a Gaussian law, see Fig. 1(b). This model relies on the definition of “asperity”. The asperity concept itself has proven to be quite controversial and depends on the resolution of the instrument used to measure the surface profile. In addition, the long range elastic coupling between the asperity contact regions is now known to strongly influence con-

tact mechanics. If an asperity is pushed downwards at a certain location, the elastic deformation field extends a long distance away from the asperity influencing the contact involving other asperities further away. This effect is neglected in the GW theory, significantly limiting its prediction capabilities when applied to most real surfaces. Additionally, in the GW model the asperity contact regions are assumed to be circular (or elliptical) while the actual contact regions (at high enough experimental resolution) show fractal-like boundary lines. Therefore, because of their complex geometries, one should try to avoid explicitly invoking the nature of the contact regions when searching for an analytical methodology to solve the contact problem of two elastic rough surfaces.

Recently, an analytical contact mechanics model that does not use the asperity concept and becomes exact in the limit of complete contact has been developed by Persson[24]. The theory accounts for surface roughness on all relevant length scales and includes (in an approximate way) the long range elastic coupling between asperity contact regions. In this theory the information about the surface enters via the surface roughness power spectrum, which depends on all the surface roughness wavevectors components.

The contact mechanics formalism developed by Persson [24] is based on studying the interface between two contacting solids at different magnifications ζ . When the system is studied at the magnification ζ it appears as if the contact area equals $A(\zeta)$, but when the magnification increases, it is observed that the contact is incomplete, and the surfaces in the apparent contact area $A(\zeta)$ are in fact only in partial contact, see Fig. 2. The theory can be used to calculate the interfacial stress distribution $P(\sigma, \zeta)$, from which one can obtain the area of real contact as a function of the squeezing pressure p and the magnification ζ . Furthermore, the theory predicts the average interfacial surface separation \bar{u} (see Ref. [25]), and the distribution of interfacial separation $P(u)$ (see Ref. [26] and [27]), which is very important for the leak-rate and friction of seals[28].

3 Friction between randomly rough surfaces

Randomly rough surfaces can be generated mathematically by adding cosine waves with different wavelength, suitable chosen amplitudes and with random phases. Such surfaces have a Gaussian height distribution and, of course, zero skewness. Real surfaces, e.g., produced by crack propagation or sandblasting, are usually nearly randomly rough surfaces.

Consider two elastic solids with randomly rough but nominal flat surfaces, squeezed into contact with the nominal pressure p . In this case, assuming linear elasticity, it has been shown both theoretically (using the Persson contact mechanics theory) and in exact numerical studies that as long as the contact area A is below $\sim 30\%$ of the nominal contact area A_0 , there is a linear

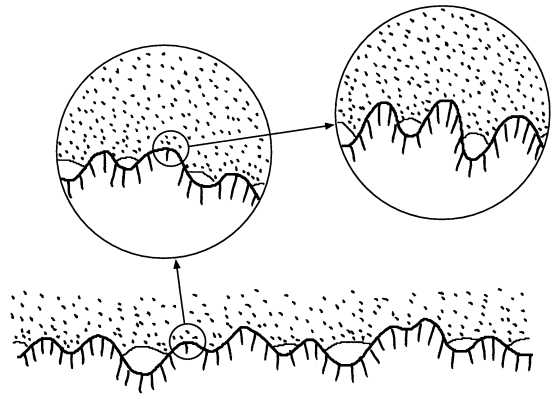


Figure 2: An elastic block (dotted area) in adhesive contact with a rigid rough substrate (dashed area). The substrate has roughness on many different length scales, and the block makes partial contact with the substrate on all length scales. When a contact area is studied, at low magnification it appears as if complete contact occurs, but when the magnification is increased it is observed that in reality only partial contact exists.

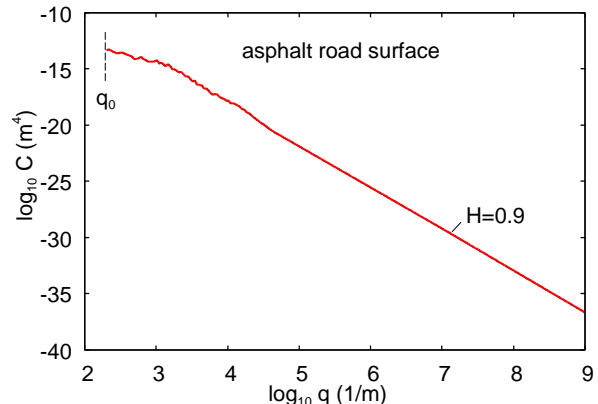


Figure 3: The surface roughness power spectrum used in the adhesion and contact mechanics calculations.

relation between the relative contact area A/A_0 and the squeezing pressure.

The physical reason for this linear relation is as follows: With increasing pressure p , existing contact areas grow and new contact areas form in such a way that, in the thermodynamic limit (infinitely large system), the (normalized) interfacial stress distribution, and also the size distribution of contact spots, are independent of the squeezing pressure. From this it follows immediately that A varies linearly with the squeezing force pA_0 . The same linear scaling will be found for any quantity that derives from the stress distributions, such as the elastic energy stored there.

The linear relation between A and p is consistent with the Coulomb friction law which states that the friction

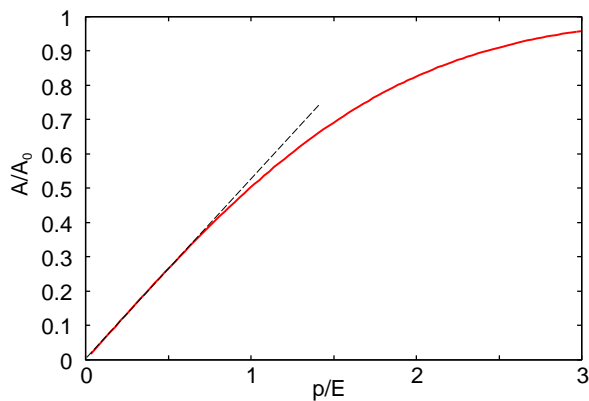


Figure 4: The area of real contact, as a function of the nominal contact pressure (in units of E), between an elastic solid with the Young's modulus E and Poisson's ratio $\nu = 0.5$, and an asphalt road surface, which is considered rigid.

force is proportional to the normal force or load: If the area of real contact is proportional to the normal force, and the normalized size distribution of contact areas independent of the load, it follows immediately that the friction force is proportional to the normal force.

Fig. 4 shows the area of real contact between an elastic solid with the Young's modulus E and Poisson's ratio $\nu = 0.5$, and an asphalt road surface. The solid line is obtained using the Persson contact mechanics theory. For pressures up to $\approx E$ the area of real contact increases linearly with the pressure p , and we expect the same for the rubber friction coefficient. For large pressures ($p > E$) the contact area approaches complete contact ($A/A_0 = 1$) and the $A(p)$ curve flattens out or saturates.

The results presented above are for an elastic solids. However, we have recently shown by exact numerical studies, and also using the Persson contact mechanics theory, that very similar results prevail for viscoelastic solids (see also next section)[29]. For viscoelastic solids the viscoelastic modulus depends on the frequency, $E = E(\omega)$, and is a complex quantity (where the imaginary part relates to energy dissipation). Since during sliding the perturbing frequencies $\omega = qv$ (where q is the wavenumber of a surface roughness component) increase with increasing sliding speed v , the relation between the contact area and the nominal contact pressure depends on the sliding speed (the contact area will decrease with increasing sliding speed). However, for any given sliding speed the area of real contact depends on the nominal contact pressure in a very similar way as for elastic solids. Hence we conclude that for the nominal contact pressures of interest in tire applications (typically $p < 0.6$ MPa) a linear relation between contact area and the nominal contact pressure can be expected.

Rubber-like materials exhibit non-linear properties, and in particular filled rubber compounds exhibit strain-softening associated with the break-up of the filler net-

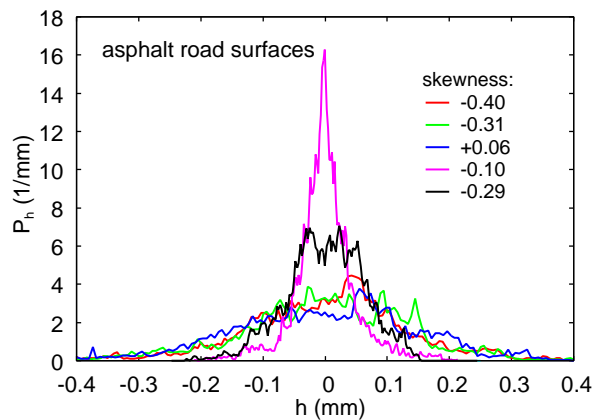


Figure 5: The surface height probability distribution for 5 different asphalt road surfaces. The average of the skewness over all 5 surfaces is $SK \approx -0.21$.

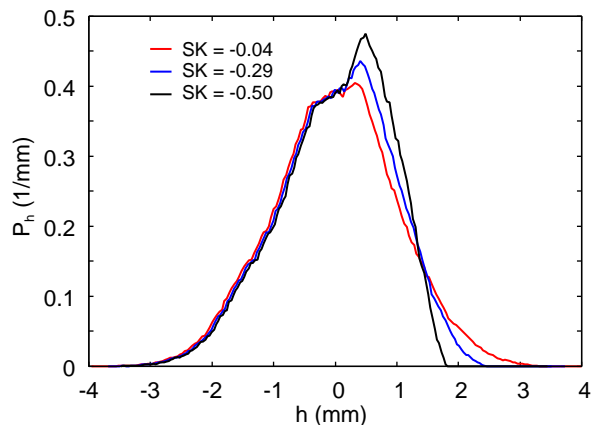


Figure 6: The surface height probability distribution for 3 mathematically generated (self-affine fractal) surfaces with the same surface roughness power spectra.

work. However, it is unlikely that this non-linearity will result in a non-linear relation between A and p for small pressures. This follows from the very general arguments given above, showing that the (normalized) distribution of stresses at the interface does not change with increasing load. Thus, most likely non-linearity in the viscoelastic properties will not change the linear relation between p and A found for linear viscoelastic solids.

4 Friction on non-randomly rough surfaces

The linear relation between contact area and the pressure expected for randomly rough surfaces at small enough load (see above), will in general not hold for surfaces with non-random roughness. This is clear already from a simple example: When a surface with a regular arranged distribution of spherical bumps, all of equal radius and height [see Fig. 1(a)], is squeezed against a flat surface, according to the Hertz contact theory, the contact area will depend non-linearly with the load as

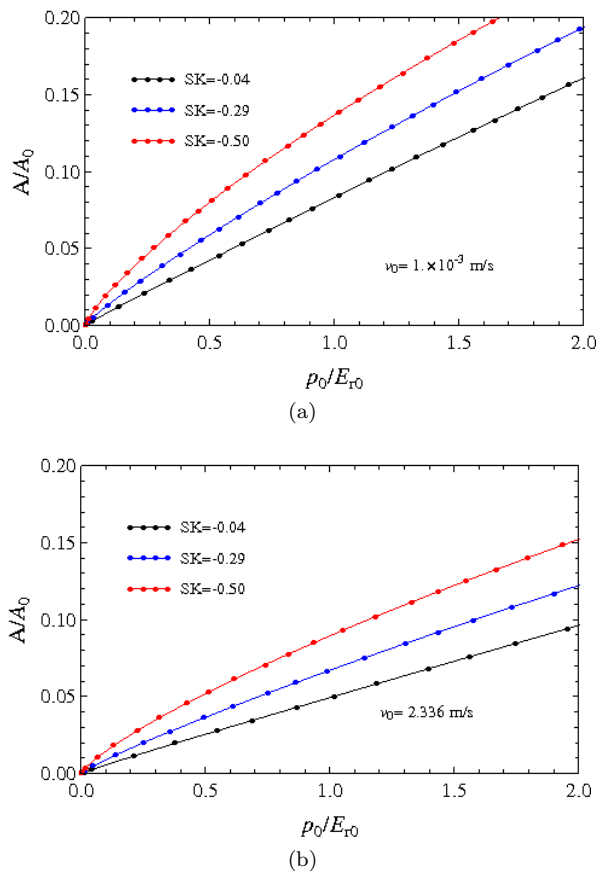


Figure 7: The normalized contact area as a function of the squeezing pressure (in units of the low frequency reduced modulus $E_{r0} = E_0/(1-\nu^2)$) as obtained from numerical calculations. Results are shown for three different surfaces with the same surface roughness power spectrum but different skewness SK . The sliding speed a) $v = 1$ mm/s, b) $v = 2.336$ m/s.

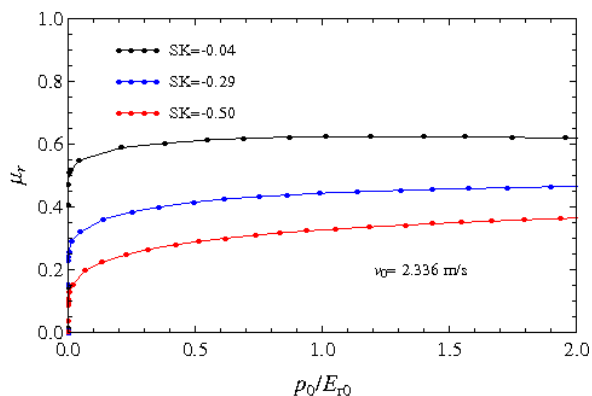


Figure 8: The viscoelastic contribution to the friction coefficient as a function of the squeezing pressure (in units of the low frequency reduced modulus $E_{r0} = E_0/(1-\nu^2)$) as obtained from numerical calculations. Results are shown for three different surfaces with the same surface roughness power spectrum but different skewness SK . The sliding speed $v = 2.336$ m/s.

$A \sim p^{2/3}$.

Asphalt road surfaces, at least when new (not extensively used), usually exhibit a negative skewness. This is a result of the production process where the hot asphalt is compressed and smoothed by rolling a heavy cylinder shaped object on the asphalt surface. This is illustrated in Fig. 5 which shows the probability distribution of surface heights of 5 different asphalt road surfaces as obtained from engineering stylus measurements. Most of the surfaces exhibit a negative skewness with the average skewness $SK = -0.21$. Surfaces with skewness are non-random, and one cannot expect such surfaces to exhibit a linear relation between p and A .

We have performed accurate numerical studies where we slide a rubber block with a flat bottom surface against hard rough surfaces with negative skewness [29, 30]. We have prepared three different surfaces with the same (self-affine fractal) power spectra, but different skewness as can be seen in Fig. 6. The skewness was produced by scaling the roughness above the average surface plane with a scaling factor < 1 to get negative skewness. In the calculations we use the viscoelastic modulus measured for a tread rubber compound, see Ref. [14].

Fig. 7(a) shows the normalized contact area as a function of the squeezing pressure (in units of the low frequency modulus E_{r0}) as obtained from the numerical calculations. Results are shown for the three different surfaces with the same surface roughness power spectrum but different skewness. The sliding speed $v = 1$ mm/s.

Fig. 7(b) shows similar results as in Fig. 7(a) but for a higher sliding speed, $v \approx 2.3$ m/s. Note that the skewness results in some non-linearity in the $A(p)$ relation for small contact pressure, and also that the contact area is larger with the skewness as compared to the case of (nearly) vanishing skewness (black data points). Both effects are easy to understand: The negative skewness implies that the surface roughness above the average plane is reduced in the height as compared to the surface with vanishing skewness. This will, for a given contact pressure, result in a larger contact area. The non-linearity in the $A(p)$ relation for small p results from the fact that at higher contact pressures the rubber penetrates deeper into the surface profile and will experience the larger roughness which exists deeper into the surface profile.

Note also that the contact area is smaller at the higher sliding speed. This is due to the higher perturbing frequencies $\omega = qv$ (see Sec. 3) acting on the rubber surface from the road asperities and to the fact that the magnitude of the viscoelastic modulus $|E(\omega)|$ increases with increasing ω .

Fig. 8 shows the viscoelastic contribution to the friction coefficient as a function of the squeezing pressure (in units of the low frequency reduced modulus $E_{r0} = E_0/(1-\nu^2)$) as obtained from the exact numerical calculations. Results are shown for the same surfaces as in Fig. 7(a) and for the sliding speed $v = 2.336$ m/s. The de-

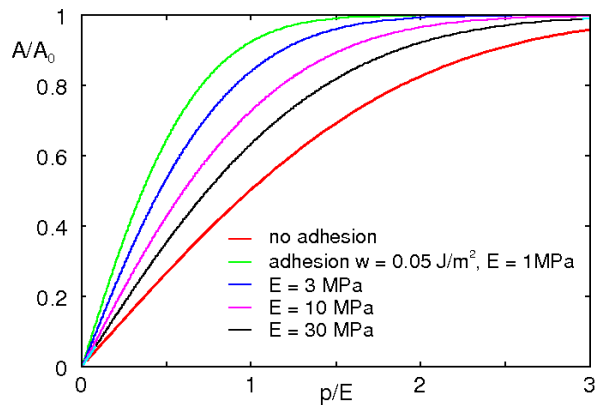


Figure 9: The area of real contact between an elastic solid with the Young’s modulus E and Poisson’s ratio $\nu = 0.5$, and a (rigid) asphalt road surface. The black line is without adhesion, and the other lines with adhesion using the work of adhesion between flat surfaces $w = 0.05 \text{ J/m}^2$, as is typical for the (adiabatic) work of adhesion between rubber and many solids (in this case the physical origin of w is usually due to the weak Van der Waals interaction).

crease in the friction coefficient with decreasing nominal contact pressure for small contact pressures is a finite-size effect, and for larger system the friction coefficient approach a constant value for small contact pressures (see Ref. [29, 30]). Note that with increasing magnitude of the (negative) skewness the friction decreases. This is again due to the fact that the surfaces above the average plane becomes smoother as the magnitude of the (negative) skewness becomes larger.

We finally note that for real asphalt road surfaces, the skewness of the surface may have much smaller influence on the contact area (and the friction) than found in the model study above. The reason for this is as follows: In our study we generate the roughness profile by scaling the roughness above the average plane on a randomly rough surface (with skewness $SK = 0$) with a factor < 1 . This will scale all asperities (big or small) with the same factor. However, asphalt road surfaces are produced by mixing stone particles of different sizes with a binder. Since the flattening of the hot asphalt, by rolling a cylinder body on top of it, will not break the stone particles it is likely that the short wavelength roughness resulting from the small stone particles will not be modified in the region above the average plane as compared to below the average plane. Only the position of the big stone particles will be modified such as to result in a smoother surface after the rolling action. But both the contact area and the rubber friction depends mainly on the shorter wavelength roughness, and will not be much affected by modification of the long wavelength roughness due to the flattening.

5 Rubber friction: role of adhesion

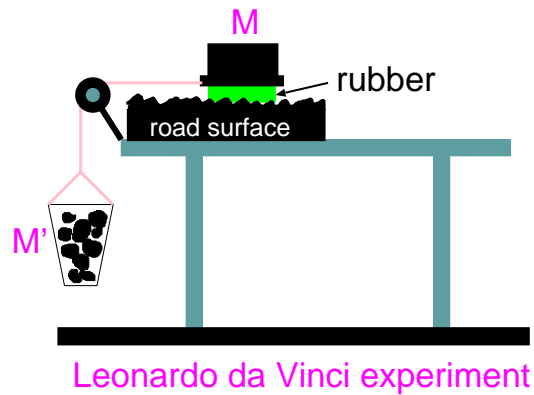


Figure 10: Simple friction tester (schematic) used for obtaining the friction coefficient $\mu = M'/M$ as a function of the sliding speed. The sliding distance is measured using a distance sensor and the sliding velocity obtained by dividing the sliding distance with the sliding time. This set-up can only measure the friction coefficient on the branch of the $\mu(v)$ -curve where the friction coefficient increases with increasing sliding speed v .

We now discuss the influence of adhesion on rubber friction and the contact area. Fig. 9 shows the area of real contact between an elastic solid with the Young’s modulus E and Poisson’s ratio $\nu = 0.5$, and an asphalt road surface with the surface roughness power spectrum $C(q)$ given in Fig. 3. The black line is without adhesion [from Fig. 4(a)], and the other lines with adhesion using the work of adhesion between flat surfaces $w = 0.05 \text{ J/m}^2$, as is typical for the (adiabatic) work of adhesion between rubber and many solids (in this case the physical origin of w is usually due to the weak Van der Waals interaction). Note that even when adhesion is included the contact area increases linearly with the nominal contact pressure, but with a slope which is larger than in the absence of adhesion.

For smoother surfaces than used above the contact area for vanishing applied load (or nominal contact pressure) may be non-zero, and the $A(p)$ relation non-linear already for small applied load. In this case the friction coefficient will depend on the load and, in particular, increase towards infinite as the load decreases towards zero. This has been observed in many experiments, but for tread rubber in contact with clean road surfaces this will not be the case because of the large surface roughness. We conclude that in tire applications, at least on clean surfaces, including adhesion will still result in a friction coefficient which is independent of the nominal contact pressure for small enough contact pressures. Nevertheless, the adhesive interaction will increase the area of real contact and the friction force.

6 Rubber friction: experimental results for low sliding speed

At low sliding speed (negligible frictional heating),

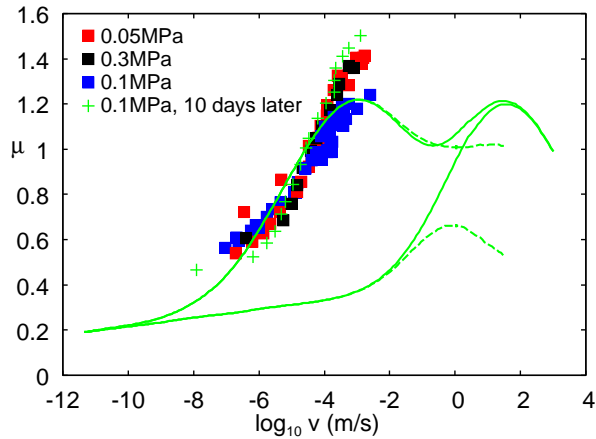


Figure 11: The measured and calculated friction coefficient as a function of sliding speed for a rubber compound on concrete surface. The upper green lines are the total calculated rubber friction coefficient and the lower green lines the viscoelastic contribution. The solid lines are without flash temperature and the dashed lines with the flash temperature. The background temperature is $T_0 = 8^\circ\text{C}$ and the nominal contact pressure $p = 0.05$ MPa (red squares), $p = 0.3$ MPa (black squares) and $p = 0.1$ MPa (blue squares and green +).

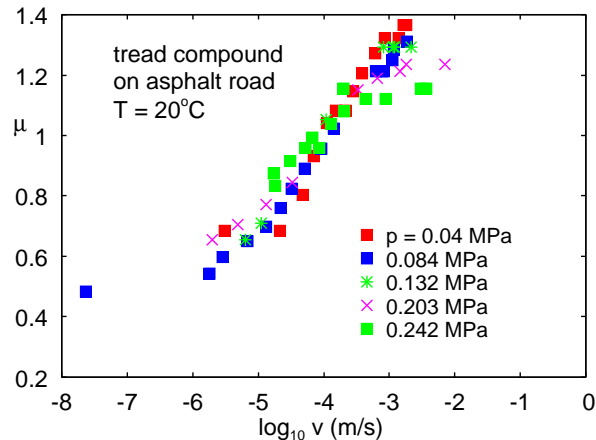


Figure 12: The measured friction coefficient as a function of sliding speed for a rubber compound on an asphalt road surface. The background temperature is $T_0 = 20^\circ\text{C}$, and for the nominal contact pressure indicated in the figure.

many experiments show that the rubber friction coefficient on rough surfaces is approximately independent of the normal load. We now report on measured rubber friction for tread rubber compounds sliding against concrete and asphalt road surfaces. The measurements were performed using the Leonardo da Vince set-up shown in Fig. 10. The slider consists of two rubber blocks glued to a wood plate. This simple friction tester can be used for obtaining the friction coefficient $\mu = M'/M$ as a function of the sliding speed. The sliding distance is measured using a distance sensor, and the sliding velocity obtained by dividing the sliding distance with the sliding time. This

set-up can only measure the friction coefficient on the branch of the $\mu(v)$ -curve where the friction coefficient increases with increasing sliding speed v , and the maximum velocity data points, in the measured data presented below, correspond to local maximum in the $\mu(v)$ curves.

Fig. 11 shows the measured and calculated friction coefficient as a function of sliding speed for a rubber tread compound on concrete (see Ref. [34] for details related to theory prediction). The nominal contact pressure $p = 0.05$ MPa (red squares), $p = 0.3$ MPa (black squares), and $p = 0.1$ MPa (blue squares and green +). The green + data was measured 10 days after the black-square measurement. During this time period the road surface and the rubber slider were both kept in the normal atmosphere. Clearly a modification of the rubber (and/or road) surface properties must have taken place. However, within the accuracy of the measurements, there is no dependency of the friction coefficient on the normal load, when the experiments are performed on surfaces the same day.

Fig. 12 shows the measured friction coefficient as a function of sliding speed for another rubber tread compound on an asphalt road surface. The results are for the background temperature is $T_0 = 20^\circ\text{C}$, and for several nominal contact pressure is indicated in the figure. For this surface it appears as if the maximum of the friction coefficient decreases with increasing nominal contact pressure. At the same time the friction coefficient for lower velocities may be slightly increased when the nominal contact pressure increases.

We now discuss why the friction coefficient in Fig. 11 may depend on the nominal contact pressure for sliding speeds $v < v_{\max}$, close to the sliding speed $v = v_{\max}$ where the friction coefficient is maximal. We assume that the contact area is proportional to the nominal contact pressure p , and that with increasing pressure p , existing contact areas grow and new contact areas form in such a way that the (normalized) interfacial stress distribution, and also the size distribution of contact spots, are independent of the squeezing pressure (see Sec. 3). In this case the only thing which could influence the sliding friction is the concentration of macroasperity contact regions which increase proportional to p .

We suggest the following picture: for velocities well below the velocity v_{\max} , where the friction coefficient is maximal in Fig. 12, the rubber in all the macroasperity contact regions slip relative to the substrate with the same velocity v as the upper surface of the rubber block. In that case the elastic (or rather viscoelastic) lateral coupling between the rubber contact regions, arising from the rubber deformation field around the asperity contact regions, is not changing in time, and it is basically irrelevant for the friction. Now, for velocities $v > v_{\max}$ the rubber friction decreases with increasing sliding speed. In the present case where the driving force is constant, this results in an accelerated motion of the rubber block when

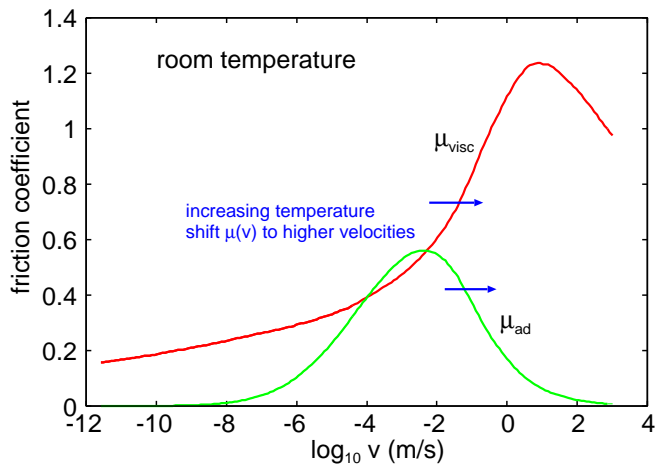


Figure 13: Schematic picture illustrating that an increase in the temperature shifts both $\mu_{\text{cont}}(v)$ and $\mu_{\text{visc}}(v)$ towards higher sliding speeds.

the driving force becomes larger than what is needed to reach the maximum in the friction coefficient. If instead the upper surface of the block would be driven with a constant velocity $v > v_{\text{max}}$ the bottom surface of the block would perform stick-slip motion. But with the same argument one expects the rubber in the macroasperity contact regions to perform stick-slip motion for $v > v_{\text{max}}$. However, due to the stochastic fluctuations in the nature of the roughness in the macroasperity contact regions one expects not a sharp onset velocity for stick-slip motion at the macroasperity level, but a distribution of onset velocities. Thus we expect that close to the friction maximum, but already for $v < v_{\text{max}}$, the individual contact regions perform stick-slip motion. In this case the shear deformation field of a macroasperity contact region depends on the shear deformation field of a nearby macroasperity contact region. Thus, we expect some correlation in the local stick-slip events when the velocity is close to the point where the friction coefficient is maximal. For example, if the rubber in a macroasperity contact region slips into a state where the shear stress vanishes, the tangential force lost in this contact region will distribute itself on the nearby rubber macroasperity contact regions, where the shear stress now may increase to the point of resulting in local slip, and so on. Clearly, this lateral coupling, and the way the stress redistribute itself in response to a local slip at a macroasperity contact region, will depend on the average separation between the macroasperity contact regions, and hence on the concentration of the macroasperity contact regions, which increases with increasing nominal contact pressure. The stick-slip events should manifest itself in the power spectrum of the block velocity or perhaps in the acoustic power spectrum, so studying these quantities should be one way to test the hypothesis presented above.

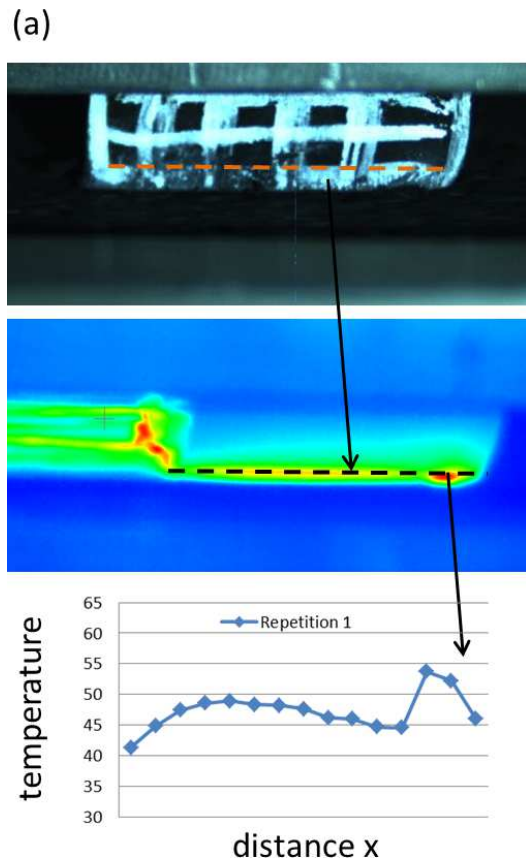


Figure 14: The measured temperature profile before run-in, after sliding $s = 3.5$ m. The rubber block is $L = 2.5$ cm long in the sliding direction and 0.7 cm high.

7 Rubber friction: role of frictional heating

There are two contributions to rubber friction, one from the viscoelastic deformations of the rubber by the road asperities[24, 33], and another from shearing the area of real contact[31, 32], the latter is usually referred to as the adhesive contribution[34]. Earlier studies have shown that at room temperature the maximum in the adhesive contribution is located below the typical slip velocities in tire applications (1 – 10 m/s), while the maximum in the viscoelastic contribution may be located above typical sliding speeds as is indicated in Fig. 13. Increasing the temperature shifts both $\mu_{\text{cont}}(v)$ and $\mu_{\text{visc}}(v)$ towards higher sliding speeds, and also increases the area of real contact A , making the adhesive contribution more important. Depending on the relative importance of the adhesive and viscoelastic contribution to the friction, the friction coefficient may increase or decrease with increasing temperatures. For passenger car tires at typical operating temperatures it appears as if the friction usually decreases with increasing temperature while for special tires, e.g., motorsport tires, the friction may increase as the temperature increases up to rather high temperatures.

The energy dissipation in the contact regions between

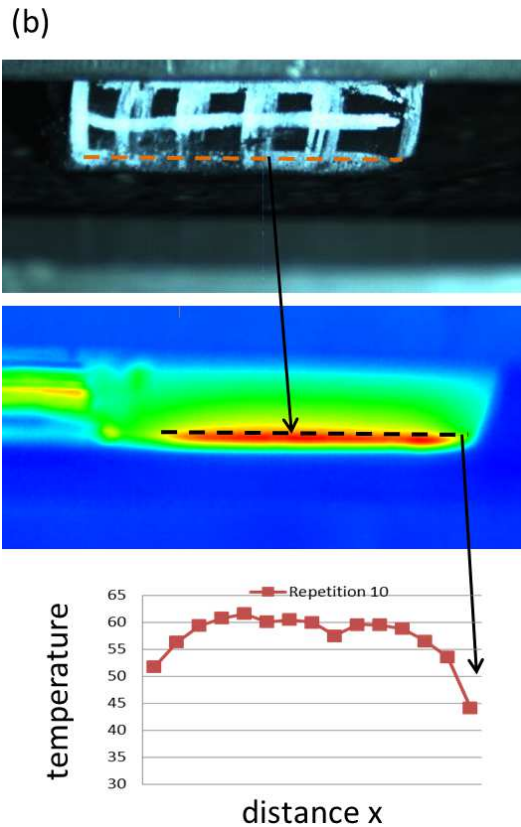


Figure 15: The measured temperature profile $T(x)$ after run-in. Run-in consists of 10 repetitions, each involving sliding of $s = 3.5$ m, i.e., a total distance of 35 m. Between each run is 10 second waiting time. The temperature profile is after the last repetition.

solids in sliding contact can result in high local temperatures which may strongly affect the contact area and the friction. This is the case for rubber sliding on road surfaces at speeds above 1 mm/s. In Ref. [14] we have derived equations which describe the frictional heating for solids with arbitrary thermal properties. Here we apply this theory to rubber friction on road surfaces, and we take into account that the frictional energy is partly produced inside the rubber due to the internal friction of rubber, and partly in a thin (nanometer) interfacial layer at the rubber-road contact region. The heat transfer between the rubber and the road surface is described by a heat transfer coefficient which depends on the sliding speed. In most cases this heat transfer coefficient is so large that the temperature basically is continuous in the contact region at the rubber-road interface, and we have made this assumption here too.

At the Bridgestone lab we have developed a rubber friction tester where a rubber block is slid on a circular asphalt road track. Using this new set-up we have studied the temperature distribution on the road surface behind the rubber block using an infrared camera.

We have found that a relatively long run-in phase is

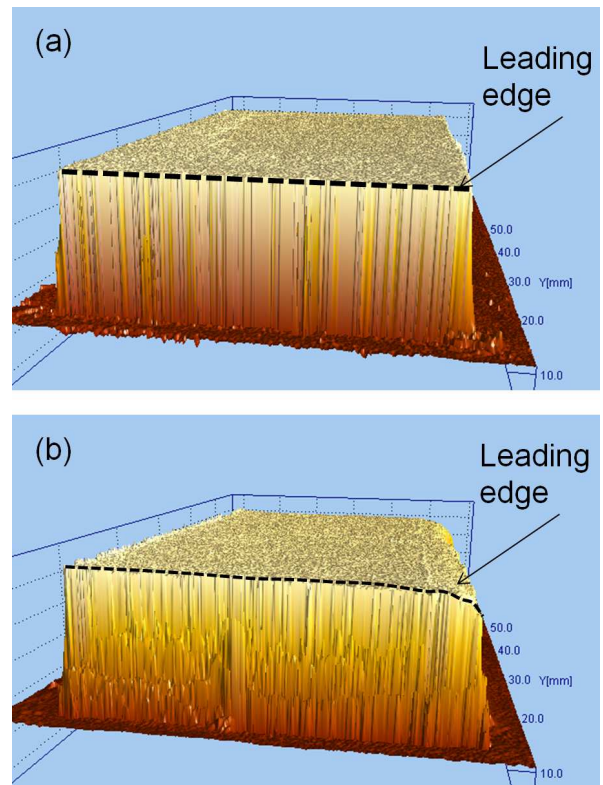


Figure 16: The measured temperature profile $T(x)$ of the rubber block (a) before run-in, (b) after run-in (10 repetitions, each involving sliding $s = 3.5$ m).

necessary in order to obtain reproducible data. During run-in the shape of the rubber block changes due to wear which results in a more uniform (nominal) contact pressure distribution. Let us first illustrate this important fact with some temperature profiles and rubber friction results.

Fig. 14 shows the measured temperature profile before run-in, after sliding $s = 3.5$ m. The rubber block is $L = 2.5$ cm long in the sliding direction, 0.7 cm high, and the nominal contact pressure is $p = 0.25$ MPa.

Fig. 15 shows the measured temperature profile after run-in. Here the run-in procedure consists of 10 repetitions, each involving sliding 3.5 m, i.e., a total of 35 m sliding distance. Between each run there is a 10 second long waiting time. The temperature profile in Fig. 15 is obtained after the last repetition.

Note that in Fig. 14 the highest temperature occurs in a very localized region close to the leading edge. Clearly before run-in the contact pressure is highly non-uniform with a maximum close to the leading edge. During run-in the high temperature and stress at the leading edge result in local wear and finally the contact pressure at the sliding interface becomes much more uniform, resulting in a more uniform temperature profile as seen in Fig. 15.

Fig. 16 shows the measured profile of the rubber block (a) before run-in and (b) after run-in (10 repetitions, each

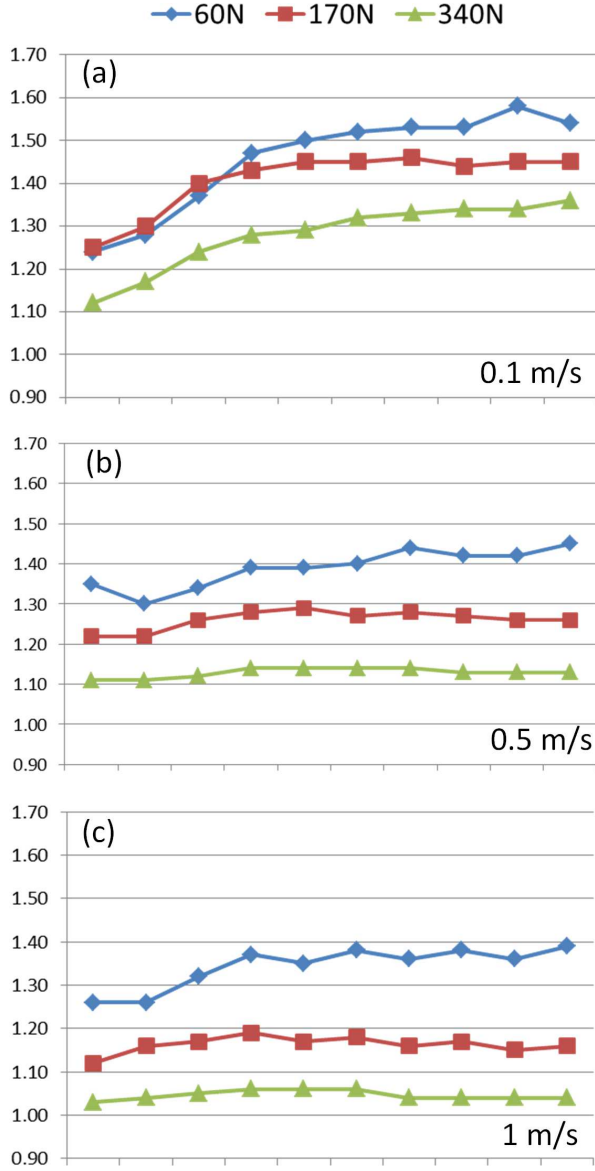


Figure 17: The measured friction coefficients as a function of the number of repetitions during run-in. Each repetition involves sliding 3.5 m at the sliding speeds (a) $v = 0.1$, (b) 0.5, and (c) 1 m/s. Results are shown for the nominal contact pressures 0.05 (blue lines), 0.15 (red), and 0.3 MPa (green).

involving sliding 3.5 m). The run-in results in a rounding off of the leading edge of the rubber block. The modification of the shape of rubber blocks during run-in has also been studied in detail by Kröger et al[35].

During run-in the rubber-road friction coefficient changes. Fig. 17 shows the measured friction coefficients as a function of the number of repetitions during run-in. Each repetition involves sliding 3.5 m at the sliding speeds (a) $v = 0.1$, (b) 0.5, and (c) 1 m/s. Results are shown for the nominal contact pressures 0.05 (blue lines), 0.15 (red), and 0.3 MPa (green). Note that the friction coefficient tends to increase with increasing number of

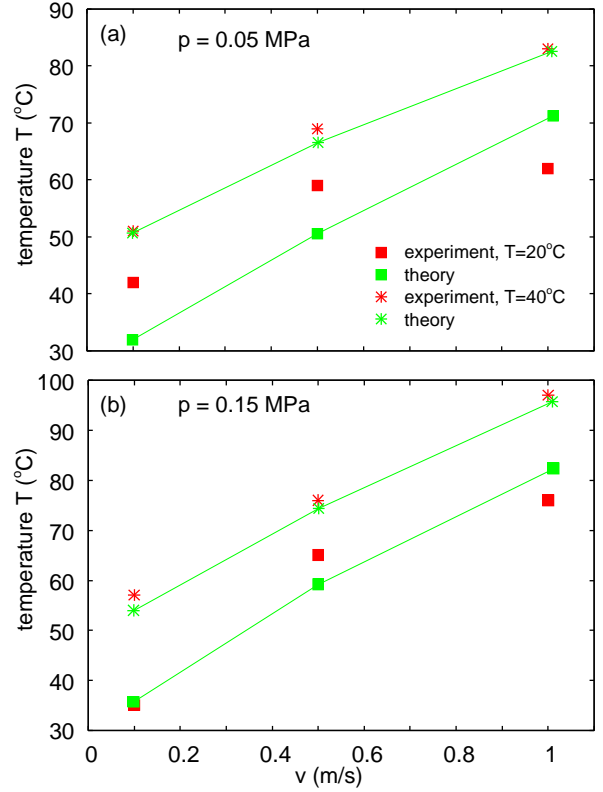


Figure 18: The measured maximal temperature on the rubber side wall (red data points) and the calculated average (over the y -direction) rubber temperature at $x = L/2$ at rubber-road interface (green symbols and lines). Results are shown when the initial temperature equals $T = 20$ and 40°C , and for the contact pressures (a) $p = 0.05$ and (b) 0.15 MPa. The block is $L = 2.5$ cm long in the sliding direction and the temperature refers to a sliding distance $s = 3.5$ m.

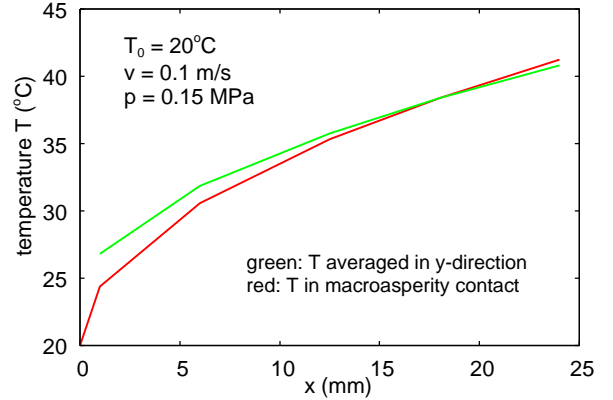


Figure 19: The calculated temperature $T(x)$ as a function of the position x along the sliding direction with $x = 0$ at the leading edge and $x = L = 2.5$ cm at the trailing edge. The temperature profile is after sliding $s = 3.5$ m at the nominal contact pressure $p = 0.15$ MPa and with the initial temperature $T = 20^\circ\text{C}$. The red line is the temperature in the macroasperity contact regions and the green line the temperature averaged over the y -direction orthogonal to the sliding direction.

run-in runs. During run-in the nominal contact pressure becomes more uniform and the local temperature increase in the region where the friction force is generated is reduced, resulting in an increase in the friction force (see below).

Let us now compare the measured temperature increase with the theory predictions. Unfortunately, the topography of the asphalt road surface track has so far only been obtained using an optical method with limited resolution, and the surface roughness power spectrum which enters in the theory calculations is therefore somewhat uncertain, in particular for large wavenumber. The theory results which we now present are obtained from the equations given in Ref. [14], and the thermal properties of the road and rubber are assumed the same as used in Ref. [14].

Fig. 18 shows the measured maximal temperature on the rubber side wall (red data points) and the calculated average (over the y -direction) rubber temperature at $x = L/2$ (middle of the nominal contact region) at the rubber-road interface (green symbols and lines). Results are shown when the initial temperature equals $T = 20$ and 40°C , for the contact pressures (a) $p = 0.05$ and (b) 0.15 MPa. The block is $L = 2.5$ cm long in the sliding direction and the temperature refers to a sliding distance $s = 3.5$ m after run-in. Note that for the lower nominal contact pressure the theory agrees almost perfectly with the measured temperature increase, while some difference occurs for the higher contact pressure.

Fig. 15 shows that the temperature in the nominal contact region is rather uniform except close to the edges of contact. As we now show this indicates that the nominal contact pressure is not quite constant, but probably increases from the trailing edge towards the leading edge, as indeed expected[36]. The reason is that if the nominal contact pressure would be constant one would expect a non-uniform temperature profile, where the temperature increases when moving from the leading edge towards the trailing edge. This is illustrated in Fig. 19.

Fig. 19 shows the calculated temperature $T(x)$ as a function of the position x along the sliding direction with $x = 0$ at the leading edge and $x = L = 2.5$ cm at the trailing edge. The temperature profile is obtained after sliding $s = 3.5$ m at the nominal contact pressure $p = 0.15$ MPa and with the initial temperature $T = 20^\circ\text{C}$. The red line is the temperature in the macroasperity contact regions and the green line the temperature averaged over the y -direction, orthogonal to the sliding direction. Note that the temperature at the leading edge is close to the road temperature, and maximal at the trailing edge. This is easy to understand: at the leading edge the rubber makes contact with a road surface, which is at the same temperature as the surrounding air (equal to the initial temperature everywhere, in this case $T = 20^\circ\text{C}$). Since the temperature is (nearly) continuous in the road-rubber asperity contact regions, the

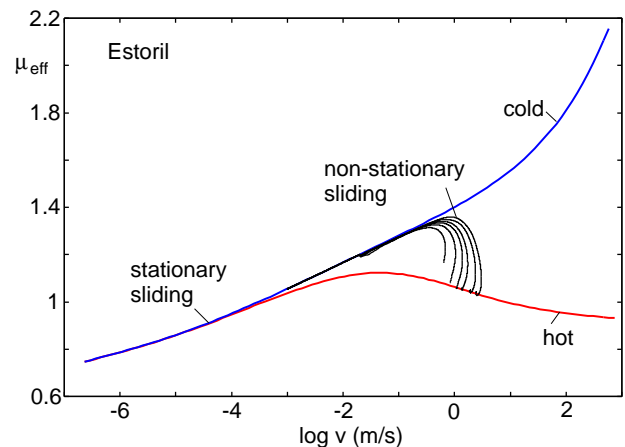


Figure 20: Red and blue lines: the kinetic friction coefficient (stationary sliding) as a function of the logarithm (with 10 as basis) of the sliding velocity. The blue line denoted “cold” is without the flash temperature while the red line denoted “hot” is with the flash temperature. Black curves: the effective friction experienced by a tread block as it goes through the footprint. For the car velocity 27 m/s and for several slip values 0.005, 0.0075, 0.01, 0.03, 0.05, 0.07, and 0.09. Note that the friction experienced by the tread block first follows the “cold” rubber branch of the steady state kinetic friction coefficient and then, when the block has slip a distance of order the diameter of the macroasperity contact region, it follows the “hot” rubber branch.

rubber temperature at the leading edge must be close to the initial road (and air and rubber) temperature. At the exit of the contact the road asperities in contact with the rubber have heated up, resulting in the maximal rubber surface temperature at the exit of the contact. Such a non-uniform temperature profile is not observed in the experiments, indicating a non-uniform nominal contact pressure. Presumably, after an even longer run-in time period, the contact pressure becomes more uniform, with the (experimental) temperature profile $T(x)$ more similar to what is predicted theoretically (see also [36]). The rather small deviation between theory and experiment in Fig. 18 is not unexpected considering that the nominal contact pressure profiles, which most likely prevail in the experiment, differ compared to the theory.

8 Implications for tire dynamics

Rubber friction depends on the history of the sliding motion. This is mainly due to the frictional heating: the temperature in the rubber-road asperity contact regions at time t depends on the sliding history for all earlier times $t' < t$. This memory effect is crucial for an accurate description of rubber friction. We illustrate this effect in Fig. 20 for a rubber tread block sliding on an asphalt road surface[3]. We show the (calculated) kinetic friction coefficient (including only the viscoelastic contribution) for stationary sliding without (blue curve) and including the flash temperature (red curve), as a function of

the velocity v of the bottom surface of the rubber block. The black curves show the effective friction during non-stationary sliding experienced by a rubber tread block during braking at various slips (slip values from 0.005 to 0.09). Note that because some finite sliding distance is necessary in order to fully develop the flash temperature, the friction acting on the tread block initially follows the blue curve corresponding to “cold-rubber” (i.e., negligible flash temperature). Thus, it is not possible to accurately describe rubber friction with just a static and a kinetic friction coefficient (as is often done even in advanced tire dynamics computer simulation codes) or even with a function $\mu(v)$ which depends on the instantaneous sliding velocity $v(t)$. Instead, the friction depends on $v(t')$ for all times $t' \leq t$.

In tire applications, for slip of order 5–10% and typical footprint length of order 10 cm, the slip distance of a tread rubber block in the footprint will be of order 1 cm, which typically is of order the diameters D of the macro asperity contact regions. As discussed above, as long as the slip distance $r(t)$ is small compared to D one follows the cold rubber branch of the steady state relation $\mu(v)$ so that $\mu(t) \approx \mu_{\text{cold}}(v(t))$ for the slip distance $r(t) \ll D$. When the tread block moves towards the end of the footprint the slip distance $r(t)$ may be of order (or larger than) D , and the friction will follow the hot branch of the $\mu(v)$ relation, i.e., $\mu(t) \approx \mu_{\text{hot}}(v(t))$ for $r(t) > D$. We have found that the following (history dependent) friction law gives nearly the same result as the full theory presented in Ref. [3, 4]:

$$\mu(t) = \mu_{\text{cold}}(v, T)e^{-r(t)/r_0} + \mu_{\text{hot}}(v, T) \left[1 - e^{-r(t)/r_0} \right] \quad (2)$$

where $v = v(t)$ is the instantaneous sliding velocity, $r(t)$ the sliding distance at time t , and $r_0 \approx 0.2D$. The background temperature T in the surface region of the rubber is assumed to be independent of the spatial coordinate.

We will refer to (2) as the *cold-hot friction law*. The length D depends on the rubber compound and the road surface but is typically in the range $D \approx 0.1\text{--}1$ cm. Using the full friction theory one can easily calculate the functions $\mu_{\text{cold}}(v, T_0)$, $\mu_{\text{hot}}(v, T_0)$, and the length D . So far, Eq. (2) has been tested when only the viscoelastic contribution is included, and the equation may need modifications when also the adhesive contribution to the friction is included in the study.

Let us illustrate the use of the cold-hot friction law (2), and the influence of the flash temperature on tire dynamics, by presenting μ -slip angle calculations for the simple 2-dimensional tire model described in Ref. [3, 4]. Fig. 21 shows the μ -slip angle curves for an elliptic footprint for the tire load $F_N = 3000, 5000$ and 7000 N, and the footprint pressure $p = 0.3$ MPa. Note that as the load increases, the footprint becomes longer which results in a decrease in the maximum friction coefficient, which agrees with experimental observations. This load-

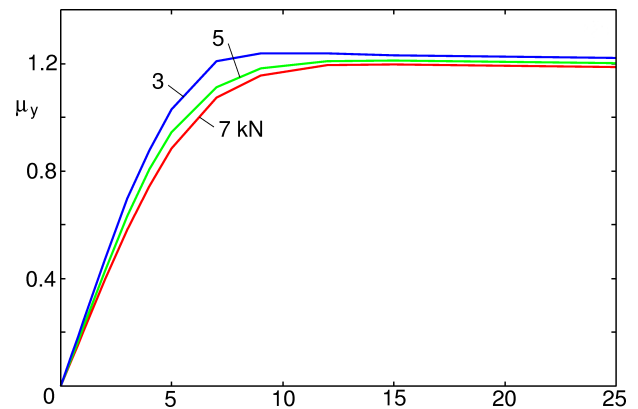


Figure 21: The μ -slip angle curves for the elliptic footprint with the tire loads $F_N = 3000, 5000$ and 7000 N, and the footprint pressure $p = 0.3$ MPa. For the rubber background temperature $T_0 = 80$ °C and the car velocity 27 m/s.

dependence is not due to an intrinsic pressure dependence of the rubber friction coefficient (which was kept constant in our calculation), but a kinetic effect related to the build up of the flash temperature in rubber road asperity contact regions during slip. To understand this in more detail, consider again Fig. 20.

The red and blue lines in Fig. 20 show the kinetic friction coefficient (stationary sliding) as a function of the logarithm of the sliding velocity. The upper line denoted “cold” is without the flash temperature while the lower line denoted “hot” is with the flash temperature. The black curves show the effective friction experienced by a tread block as it goes through the footprint. Note that the friction experienced by the tread block first follows the “cold” rubber branch, and then, when the block has slipped a distance of order the diameter D of the macroasperity contact region, it follows the “hot” rubber branch. Based on this figure it is easy to understand why the maximum friction coefficient increases when the length of the footprint decreases: If v_{slip} is the (average) slip velocity of the tread block, then in order to fully build up the flash temperature the following condition must be satisfied: $v_{\text{slip}}t_{\text{slip}} \approx D$, where D is the diameter of the macroasperity contact region. Since the time the rubber block stays in the footprint $t_{\text{slip}} = L/v_R$ (where L is the length of the footprint and v_R the rolling velocity) we get $v_{\text{slip}} \approx v_R(D/L)$. Thus, when the length L of the footprint decreases, the (average) slip velocity of the tread block in the footprint can increase without the slip distance exceeding the diameter D of the macro asperity contact region. As a consequence, as L decreases, the tread block will follow the “cold” rubber branch of the (steady state) μ -slip curve to higher slip velocities before the flash temperature is fully developed, resulting in a higher (maximal) tire-road friction for a short footprint as compared to a longer footprint.

9 Summary and conclusion

We have discussed several different origins for why μ could depend on the nominal pressure, thus violating the first Amonton's friction law. Possible explanations are: (a) saturation of the contact area (and friction force) due to high nominal squeezing pressure, (b) non-linear viscoelasticity, (c) non-randomness in the surface topography, and in particular the influence of the skewness of the surface roughness profile, (d) adhesion and (e) frictional heating.

We have shown that for most cases the non-linearity in the $\mu(p)$ relation is mainly due to process (e) (frictional heating). This is for example the case for a tire in contact with the road surface where the contact area is usually just a small fraction of the nominal contact area. Here the energy dissipation in the contact regions between solids in sliding contact can result in high local temperatures which may strongly affect the area of real contact and the friction force (and the wear rate). This is usually observed for rubber sliding on road surfaces at speeds above 1 mm/s. In this paper we have presented and compared numerical results to experimental data for the temperature increase of a rubber block in sliding contact with a randomly rough surface. We observe good agreement between the calculated and measured temperature increase.

Rubber friction depends very sensitively on the rubber temperature shifting the viscoelastic and the contact area contribution towards higher sliding speeds with increasing temperature, usually resulting in a decrease of the friction coefficient. When the load (or nominal contact pressure) increases, the effect of frictional heating increases as well, resulting in even higher temperatures and a non-linear dependency of the friction force on the applied normal load.

However, depending on the system studied, the non-linear relation of $\mu(p)$ can also be attributed to a saturation of contact area with normal load or to skewness of the roughness profile affecting the rubber friction. The area of real contact between elastic (or viscoelastic) solids with nominally flat, but randomly rough surfaces is usually proportional to the applied normal force as long as the area of real contact is less than $\sim 30\%$ of the nominal contact area. When the load (or nominal force) becomes so high that the contact area exceeds $\sim 30\%$ of the nominal contact area, the friction force starts to depend non-linearly on the load.

An increase of the normal load on surfaces with a skewed height profile will make the rubber surface penetrate deeper into the roughness profile, where it will experience roughness components with different statistical properties. This will influence the area of contact and also the viscoelastic contribution to rubber friction. The effect gets enhanced when frictional heating becomes high enough, leading to a softening of the rubber, an even deeper penetration of the rubber into the roughness pro-

file, and (for surfaces with negative skewness) a reduction of the viscoelastic contribution to the friction.

-
- [1] E. Rabinowicz, *Friction and Wear of Materials*, Wiley; 2nd Edition (1995).
 - [2] B.N.J. Persson, *Sliding Friction: Physical Principles and Applications*, Springer; 2nd edition (2000).
 - [3] B.N.J. Persson, *J. Phys.: Condens. Matter* **23**, 015003 (2011).
 - [4] M. Selig, B. Lorenz, D. Henrichmüller, K. Schmidt, A. Ball and B.N.J. Persson, *Tire Science and Technology* **42**, 216 (2015).
 - [5] J.C. Jaeger, *Journal and Proceedings of the Royal Society of New South Wales* **76**, 203 (1942)
 - [6] J.F. Archard, *Wear* **2**, 438 (1959).
 - [7] R. Holm, *Journal of Applied Physics* **19**, 361 (1948).
 - [8] H. Block, *Wear* **6**, 483 (1963).
 - [9] D.G. Bansal and J.L. Streato, *Wear* **278-279**, 18 (2012).
 - [10] C. Putignano, J. Le Rouzic, T. Reddyhoff, G. Carbone and D. Dini, *Proceedings of the Institution of Mechanical Engineers, Part J: Journal of Engineering Tribology*, **228**, 1112 (2014).
 - [11] Y. Liu and J.R. Barber: *Transient Heat Conduction Between Rough Sliding Surfaces. Tribol. Lett.* **55**, 23 (2014).
 - [12] B.N.J. Persson, *J. Phys.: Condens. Matter* **18**, 7789 (2006).
 - [13] B.N.J. Persson, *Tribol. Lett.* **56**, 77 (2014).
 - [14] G. Fortunato, V. Ciaravola, A. Furno, B. Lorenz, B.N.J. Persson, *JOURNAL OF PHYSICS-CONDENSED MATTER* **27**, 175008 (2015).
 - [15] K.G. Rowe, A.I. Bennet, B.A. Krick and W.G. Sawyer, *Tribology International* **62**, 208 (2013).
 - [16] B.N.J. Persson, B. Lorenz and A.I. Volokitin, *Eur. Phys. J.* **E31**, 3 (2010)
 - [17] B.N.J. Persson, A.I. Volokitin and H. Ueba, *J. Phys.: Condens. Matter* **23** 045009 (2011)
 - [18] B.N.J. Persson, *J. Phys.: Condens. Matter* **26**, 015009 (2014).
 - [19] J.R. Barber, *Proc. R. Soc. London, Ser. A* **459**, 53 (2003).
 - [20] J.A. Greenwood, *Brit. J. Appl. Phys.* **17**, 1621 (1966).
 - [21] C. Campana, B.N.J. Persson and M.H. Müser, *J. Phys.: Condens. Matter* **23**, 085001 (2011).
 - [22] L. Pastewka, N. Prodanov, B. Lorenz, M. H. Müser, M. O. Robbins, and B. N. J. Persson, *Phys. Rev. E* **87**, 062809 (2013)
 - [23] K.L. Johnson, *Contact mechanics*, Cambridge university press (1987).
 - [24] B.N.J. Persson, *J. Chem. Phys.* **115**, 3840 (2001).
 - [25] B.N.J. Persson, *Phys. Rev. Lett.* **99**, 125502 (2007).
 - [26] A. Almqvist, C. Campana, N. Prodanov and B.N.J. Persson, *Journal of the Mechanics and Physics of Solids* **59**, 2355 (2011).
 - [27] C. Yang and B.N.J. Persson, *J. Phys.: Condens. Matter* **20**, 215214 (2008).
 - [28] W.B. Dapp, A. Lücke, B.N.J. Persson, and M.H. Müser *Self-Affine Elastic Contacts: Percolation and Leakage*, *Phys. Rev. Lett.* **108**, 244301 (2012)
 - [29] M. Scaraggi and B.N.J. Persson, *J. Phys.: Condens. Matter* **27**, 105102 (2015).

- [30] M. Scaraggi and B.N.J. Persson, unpublished
- [31] A. Schallamach, *Wear* **6**, 375 (1963)
- [32] B.N.J. Persson and A.I. Volokitin, *Eur. Phys. J. E* **21**, 69-80 (2006)
- [33] M. Klüppel and G. Heinrich, *Rubber Chem. Technol.* **73**, 578 (2000).
- [34] B. Lorenz, Y.R. Oh, S.K. Nam, S.H. Jeon and B.N.J. Persson, *The Journal of chemical physics* **142**, 194701 (2015).
- [35] G. Gäbel and M. Kröger, VDI-Berichte Nr. 2014 (2007) Page 245-259; G. Gäbel, P. Moldenhauer and M. Kröger, *ATZ* 06I2008 Jahrgang 110, 562.
- [36] See, e.g., PhD thesis of P. Moldenhauer, *Modellierung und Simulation der Dynamik und des Kontakts von Reifenprofilblöcken* (2010).

